

#### Contents lists available at ScienceDirect

#### Mechatronics

journal homepage: www.elsevier.com/locate/mechatronics





## Identification of an overactuated deformable mirror system with unmeasured outputs $^{, \star, \star \star}$

Paul Tacx a,\*, Roel Habraken a,b, Gert Witvoet a,b, Marcel Heertjes a,c, Tom Oomen a,d

- <sup>a</sup> Department of Mechanical Engineering, Eindhoven University of Technology, Eindhoven, The Netherlands
- <sup>b</sup> TNO, Optomechatronics Department, Delft, The Netherlands
- <sup>c</sup> ASML, Mechatronic Systems Development, Veldhoven, The Netherlands
- <sup>d</sup> Faculty of Mechanical, Maritime, and Materials Engineering, Delft University of Technology, Delft, The Netherlands

#### ARTICLE INFO

# Keywords: Adaptive optics Local parametric modeling Modal analysis Motion control Mechanical models Mechatronics

#### ABSTRACT

Next-generation deformable mirrors are envisaged to exhibit low-frequency flexible dynamics and to contain a large number of spatially distributed actuators due to increasingly stringent performance requirements. The increasingly complex system characteristics necessitate identifying the flexible dynamic behavior for design validation and next-generation control. The aim of this paper is to develop a unified approach for the identification of mechanical systems with a large number of spatially distributed actuators and a limited number of sensors. A frequency domain-based approach using local modeling techniques is developed. The modal modeling framework is employed to analyze the design and create outputs that were not measured. The proposed approach is applied to an experimental deformable mirror case study that illustrates the effectiveness of the proposed approach.

#### 1. Introduction

#### 1.1. Background

Adaptive optics (AO) is increasingly important in ground-based astronomy due to increasingly stringent image quality requirements [1-3]. Wind and thermal variations in the atmosphere cause atmospheric turbulence that in turn leads to wavefront (WF) distortions [4]. Adaptive optics are employed to recover the incoming wavefront, see Fig. 1. A wavefront sensor (WFS), typically a Shack-Hartmann sensor, is used to measure the gradient of the wavefront at a finite number of points [5]. The wavefront is then reconstructed from the gradient information. A deformable mirror is used to compensate for wavefront distortions by a large number of spatially distributed actuators that enable the deformation of the performance surface. Due to developments in astronomy, next-generation deformable mirrors are expected to increase in complexity for two main reasons [1]. First, the effect of atmospheric disturbances expressed by wavefront distortions becomes more pronounced due to the trend of increasing primary mirror dimensions in ground-based observatories. An increased number of spatially distributed actuators is required to compensate for this effect. Second,

increasing imaging quality demands requires the deformable mirror to be located early in the optical path, hence, next-generation deformable mirrors will act as the secondary mirror in the telescope, i.e. adaptive secondary mirrors, which requires an increased deformable mirror diameter. As a consequence of the increased mirror diameter, future deformable mirrors predominantly exhibit flexible dynamic behavior at lower frequencies [6].

The presence of flexible dynamics at low frequencies in next-generation deformable mirrors impacts the analysis and control of deformable mirrors [7,8]. First, for traditional small deformable mirrors, the flexible dynamic behavior occurs beyond the control bandwidth. For this reason, the deformable mirror dynamics are assumed to be static over frequency and that each actuator only has a local influence on the performance surface. This allows the construction of a so-called static influence function, which is a frequency-independent map from the actuator to the surface deformation [9,10]. However, for future deformable mirror systems, that are expected to be significantly larger, these assumptions are no longer valid due to the flexible dynamic behavior at low frequencies. Consequently, the structural dynamics need to be addressed explicitly in the design and control architecture

E-mail address: p.j.m.m.tacx@tue.nl (P. Tacx).

This work is part of the research programme VIDI with project number 15698, which is (partly) financed by The Netherlands Organization for Scientific Research (NWO).

<sup>&</sup>lt;sup>☆☆</sup> This paper was recommended for publication by Associate Editor Zheng Chen.

<sup>\*</sup> Corresponding author.

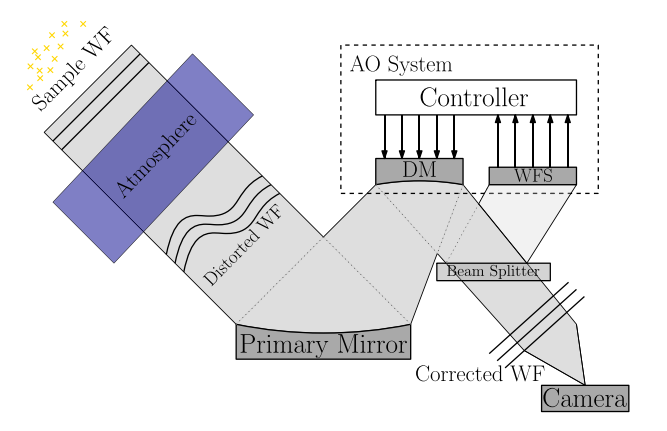


Fig. 1. Schematic overview of an adaptive optics systems integrated into a telescope.

which requires accurate dynamical models of the flexible dynamic behavior [11,12]. Second, to validate the next-generation designs, models are required to analyze and provide insight into the mechanical behavior.

#### 1.2. Problem formulation

The increasingly complex dynamics in next-generation deformable mirrors necessitate modeling approaches that explicitly target the flexible dynamic behavior. However, traditional modeling approaches for control of deformable mirrors consider their temporal response to be static and thus ignore their flexible dynamic behavior [13-16]. If the deformable mirror system is integrated into a telescope, the large grid of the wavefront sensor is often used for system identification [9]. However, this approach is not tenable for next-generation deformable mirrors, as it is desirable to validate their design on component level before integration, i.e., when the main wavefront sensor is not yet available. Alternatively, a temporary optical setup with a wavefront sensor can be considered [17,18]. However, such setups are large, expensive, and simple wavefront sensors often lack a sufficiently high bandwidth to capture the flexible dynamic behavior. Thus, an identification approach is required for identifying models for design validation and control design of overactuated systems with a limited number of temporary position and acceleration sensors. At the same time, the identification approach should enable accurate modeling with limited experiment time. Moreover, the models should provide physical insights into the flexible behavior.

#### 1.3. Literature survey

Several approaches have been pursued to identify the flexible dynamic behavior of deformable mirrors including finite-element-based methods. In [7,19–21], a numerical modal analysis of a deformable mirror is considered for control and analysis. However, numerical studies, such as Finite Element Method (FEM) simulations, may not be truly representative of the real system due to the high system complexity. Additionally, this method does not extend to the situation of integration into the telescope, as the suspension of the deformable mirror is not always known in advance.

A first-principles-based modeling approach is used as an alternative to FEM-based techniques to identify overactuated mechatronic systems in [22,23]. However, the considered approach heavily relies on single two-dimensional plate theory, which may not be accurate enough to capture the complex dynamics of the three-dimensional structure. In [24–26], a method is proposed to estimate the parameters of a partial differential equation-based model of the performance surface of a deformable mirror. However, these approaches only consider the dynamics of the performance surface and therefore miss the fidelity

to describe the dynamics of the entire deformable mirror structure, e.g., actuator support structure. Consequently, these first-principles-based approaches do not give insight into the underlying dynamics of the support structure. Additionally, during system integration, modeling is often time-critical, which motivates an experiment-based approach for the modeling of generic mechatronic systems, including deformable mirrors.

Experimental identification approaches tailored to deformable mirrors are considered in [9,10]. However, these approaches only consider the static system behavior at low frequencies and are therefore not suitable to model the flexible dynamic system behavior.

An experiment-based approach through Frequency Response Function (FRF) estimates is often used for analysis and control of mechatronic systems, see e.g. [10,27–29]. However, when traditional spectral analysis is used, a significant amount of measurement time is required, especially for systems with a large number of actuators. Local parametric methods can be used to reduce measurement time and enhance the quality of FRF estimates [30,31]. Local parametric methods have been successfully applied to mechatronic systems in several studies, such as [29,32]. In [33], the Local Rational Method (LRM) is applied to MIMO systems with a large number of inputs and outputs in a simulation environment with promising results. A limitation of FRF estimates is that these become complicated to interpret if the number of elements inflates by increasing the number of inputs and outputs. This limits practical insight into the flexible dynamics.

Parametric models are important for control of many mechatronic applications including, e.g., astronomy, aerospace, and lithography [29, 34,35]. In particular, modal models of these mechanical systems lead to practically interpretable results that are also useful for control [36,37]. In addition, a method for identifying position-dependent modal models of mechatronic systems based on frequency response function estimates is presented in [29]. These results are tailored for motion control of systems that consist of a single moving body which is not valid for the class of deformable mirrors that are considered in this paper. Moreover, the analysis is tailored to the limited number of sensor locations which limits insight into the underlying flexible dynamics.

Alternatively, the field of structural engineering and modal analysis often deals with systems with a large number of inputs to analyze a system through the roving hammer survey. In [38], an identification approach is proposed tailored to vibration isolation control of flexible building structures. The method relies on a limited number of sensors and an impact hammer is used at various locations to excite the system. The concept of reciprocity allows the interpretation of the additional excitation locations as fictitious sensors which allows for enhanced insights into the underlying system dynamics [39-41]. However, for high-tech applications, including deformable mirror systems, an impact hammer may damage the system and is therefore not preferred. Alternatively, the actuators of a mechanical system can be used to create additional fictitious sensors. Such an approach is suggested in [42], but it assumes a rigid actuator support structure, i.e., absolute actuation. However, the deformable mirrors considered in this paper have two flexible bodies due to the relative actuation caused by the flexible support structure, i.e., backplate. As a consequence, the proposed method is not directly applicable to this class of deformable mirrors.

#### 1.4. Scope and contribution

Although several techniques (as discussed above) are available for the analysis of mechanical systems in the field of mechatronics, at present, these tools are not tailored to systems with a large number of actuators and a limited number of sensors such as deformable mirrors.

The main contributions of this paper are the following.

C1 A frequency response identification approach and its experimental application on overactuated systems with a limited number of sensors.

- C2 A unified modal model identification approach through fictitious sensors for the analysis of overactuated systems with a limited number of sensors.
- C3 A simulation case study to illustrate the proposed tools.
- C4 An experimental case study with an experimental deformable mirror setup including a design analysis using the proposed tools.

Existing experimental methods for identifying deformable mirrors assume static system behavior and are therefore not suitable for design analysis and control of deformable mirrors that exhibit flexible dynamics within the control bandwidth [13–16]. Existing identification methods that do consider the flexible dynamic behavior are typically based on simulation models [22–26]. In sharp contrast, the approach in this paper is based on experiments. In particular, the approach does not rely on prior system knowledge, advanced modeling techniques, and it requires limited experiment time and limited user intervention. Lastly, in contrast to many results in the literature that consider simulation case studies, in this paper, the proposed approach is applied in an experimental case study with a deformable mirror.

A frequency domain-based approach is pursued to identify the flexible dynamic behavior. Compared to a time domain-based approach, e.g., [38], a frequency domain-based approach is data-efficient, facilitates practical interpretation, and provides an efficient starting point for parametric modeling. Specifically, an approach using the local rational method is developed since it allows for accurate and fast non-parametric identification. Compared to conventional non-parametric system identification approaches, e.g., [43], the local parametric method requires significantly less experiment time. However, to the authors' best knowledge, the local parametric method has not yet been used in an experimental setting with a large number of inputs and outputs.

Based on the frequency response function estimate, an approach to identify modal models is developed. Compared to existing optimization-based approaches, e.g., [29], the approach considered in this paper is relatively simple and therefore requires less user intervention. Unmeasured outputs are estimated to enhance insight into the underlying structural dynamics. The key idea is that the large number of spatially distributed actuators can be used as fictitious sensors by exploiting the modal system description. Compared to conventional structural analysis approaches, this approach does not require an impact hammer. Also, the method proposed in this paper extends to the approach in [42] by generalizing it to overactuated systems, including deformable mirror systems, that have a flexible actuator support structure.

#### 1.5. Organization of the paper

The paper is organized as follows. In Section 2, the main application considered in this paper and the problem formulation are discussed. In Section 3, the FRF estimation procedure is introduced. The modal identification is described in Section 4. An experimental case study with an experimental deformable mirror is presented in Section 5. Conclusions are provided in Section 6.

#### 1.6. Notation

The following notation is used throughout. For a matrix  $A \in \mathbb{R}^{n \times m}$ , the singular value decomposition is given by  $A = U \Sigma V^{\top}$ , where U is an  $m \times m$  orthogonal matrix,  $\Sigma$  is an  $m \times n$  diagonal matrix with non-negative real entries, and V is an  $n \times n$  orthogonal matrix.

The transfer function matrix, denoted by G(s), represents the relationship between the input and output signals of a linear multivariable system in the frequency domain. The variable s is the complex Laplace variable. For a matrix A, the transpose and complex conjugate transpose are denoted by  $A^{\top}$  and  $A^*$  respectively.

#### 2. Problem formulation

#### 2.1. Motivation

Stringent requirements regarding image quality have led to the development of a next-generation deformable mirror design. This paper is specifically focused on a unique class of deformable mirrors capable of replacing the secondary mirror, offering a distinct advantage of improved image quality compared to deformable mirrors positioned further along the optical path. Distinguished by their larger size and relatively wide actuator spacing, these deformable mirrors deviate from conventional designs commonly found in smaller systems such as those from ALPAO and OKO, where piezoelectric-based or microelectromechanical-based deformable mirrors are often used [23,44]. Due to their limited stroke, these piezoelectric actuators are unsuitable for the class of deformable mirrors considered in this paper.

Traditionally, Lorentz actuators are used in deformable mirrors for secondary mirror replacement [22]. However, a key drawback is the significant heat dissipation. Preliminary studies have demonstrated the potential of reluctance actuators in deformable mirrors [10]. Currently, such a deformable mirror is in production for the UH88 telescope with 217 actuators and a diameter of 630 mm, see Fig. 2. Also, a deformable mirror is in development for the EST with 2000 actuators and an increased diameter of 860 mm [45]. The main benefit of reluctance actuators over alternative actuation concepts such as e.g. Lorentz actuators, is the reduced dissipation around the secondary mirror and a consequent reduction in cooling requirements.

The increased size of these deformable mirrors leads to flexible dynamics at a lower frequency, within the control bandwidth, posing challenges for mechatronic design and control. For this reason, this paper focuses on the analysis and understanding of the flexible dynamics of the deformable mirror, i.e., the component level of the adaptive optics system. The key idea is to verify the flexible dynamics by identifying a suitable model for validation of the design. Ultimately, the developed model could be employed for control purposes.

A complicating aspect arises from the lack of internal sensors that measure the deformation of the deformable mirror itself at the component level, i.e., when the main wavefront sensor is not yet available. A temporary optical setup with a wavefront sensor is not considered since such setups are large, expensive, and simple wavefront sensors often lack a sufficiently high bandwidth to capture the flexible dynamic behavior. For this reason, only a limited number of temporary position and acceleration sensors are available. Consequently, there is limited access to sensor data while striving to gain a comprehensive understanding of the deformable mirror's flexible dynamics. Hence, this underlines the importance of identifying a model suitable for overactuated mechatronic systems with a limited number of sensors, enabling a complete view of the flexible dynamics.

#### 2.2. System description

Fig. 3 depicts a one-dimensional overview of an overactuated mechatronic system that is representative for the class of deformable mirrors considered in this paper. The key point is that the system contains two flexible bodies, i.e., the performance surface and the actuator backplate, which are connected by flexible elements that are part of the actuator design [10]. The connection of the backplate to the fixed world is indicated by two springs.

A complicating aspect is that the actuator backplate has a finite stiffness. As a consequence, the increasingly large dimensions of next-generation mechatronic systems result in significant low-frequency flexible dynamics that propagate to the performance surface. This can lead to problems with control and stability, as well as image quality.

The key functions of the system are the out-of-plane deformation of the performance surface,  $u_{\rm ps}(\rho,t): S_{\rm ps} \times T \mapsto \mathbb{R}$ , and the backplate,  $u_{\rm bp}(\rho,t): S_{\rm bp} \times T \mapsto \mathbb{R}$ , which are modeled as a continuum. The time domain is denoted by  $T \in \mathbb{R}$ . The two-dimensional geometries of the performance surface and backplate are denoted by the spatial domains  $S_{\rm ps} \subset \mathbb{R}^2$  and  $S_{\rm bp} \subset \mathbb{R}^2$ , respectively.



Fig. 2. Deformable mirror of the UH.88 telescope designed by TNO.

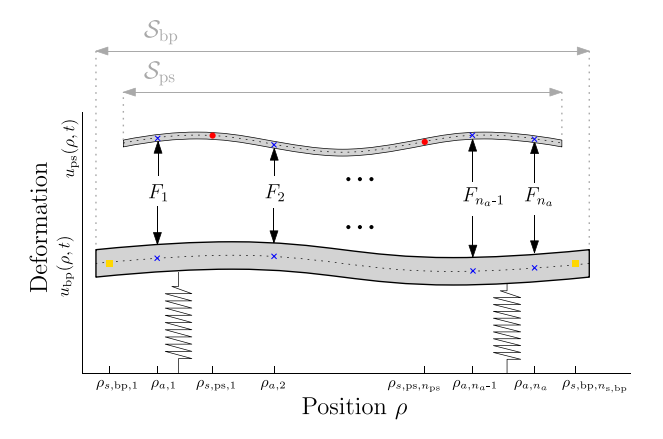


Fig. 3. One-dimensional schematic representation of a deformable mirror. The representation includes  $n_a$  actuators  $(\times)$  that are denoted as  $F_i$ ,  $i \in \{1, \dots, n_a\}$ ,  $n_{s,bp}$  sensors on the backplate ( $\blacksquare$ ), and  $n_{s,ps}$  sensors on the performance surface ( $\blacksquare$ ). The geometry of the performance surface and backplate are denoted by the spatial domains  $S_{ps}$  and  $S_{pp}$ . The performance surface and the backplate are considered to be flexible and their deformations are denoted by  $\tilde{u}_{ps}(\rho,t)$  and  $\tilde{u}_{bp}(\rho,t)$  respectively. The connection of the backplate to the fixed world is denoted by two springs at the ends of the backplate.

#### 2.3. Problem formulation

Measurement data is obtained at a finite number of spatially distributed sensor locations with a large number of spatially distributed actuators

$$g(t): f(t) \mapsto u(t) \tag{1}$$

where g(t) denotes the mechatronic system,  $f(t) \in \mathbb{R}^{n_a}$  denotes the actuator forces, and  $\bar{u}(t) \in \mathbb{R}^{n_{s,ps}+n_{s,bp}}$  the deformation measured at the sensors. The number of actuators is denoted by  $n_a$  and the locations of the actuators denoted by

$$\rho_{a,i} \subset (S_{bp} \cap S_{ps}), i = 1, \dots, n_a.$$
(2)

The geometries of the performance surface and backplate do not necessarily coincide, as illustrated in Fig. 3. For this reason, the actuator locations are restricted to the intersection of these domains. To facilitate transparency of the results, these positions are stacked into a vector

$$\rho_{\mathbf{a}} = \left[\rho_{\mathbf{a},1}, \dots, \rho_{\mathbf{a},n_{\mathbf{a}}}\right]^{\mathsf{T}}.\tag{3}$$

The sensor data is obtained with  $n_{\rm s,ps}$  sensors that measure the deformation of the performance surface

$$\bar{u}_{ps}(t) = \begin{bmatrix} u_{ps}(\rho_{s,ps,1}, t) & \dots & u_{ps}(\rho_{s,ps,n_{s,ps}}, t) \end{bmatrix}^{\mathsf{T}}$$
 (4)

and the locations of these sensors are stacked into a vector

$$\rho_{\text{S,DS},i} \in S_{\text{DS}}, \quad i = 1, \dots, n_{\text{S,DS}} \tag{5}$$

$$\rho_{s,ps} = \left[\rho_{s,ps,1}, \dots, \rho_{s,ps,n_{s,ps}}\right]^{\mathsf{T}}.$$
(6)

A limited number  $n_{s,\mathrm{bp}}$  of sensors measure the deformation of the backplate

$$\bar{u}_{bp}(t) = \begin{bmatrix} u_{bp}(\rho_{s,bp,1}, t) & \dots & u_{bp}(\rho_{s,bp,n_{s,bp}}, t) \end{bmatrix}^{\mathsf{T}}$$

$$(7)$$

at the locations that are stacked into a vector

$$\rho_{s,bp,i} \in S_{bp}, \quad i = 1, \dots, n_{s,bp}$$
(8)

$$\rho_{s,bp} = \left[\rho_{s,bp,1}, \dots, \rho_{s,bp,n_{s,bp}}\right]^{\mathsf{T}}.$$
(9)

As a consequence, a limited number of sensors measure the absolute deformation of the performance surface and the backplate. In sharp contrast, the actuation is relative between the backplate and the performance surface.

The key problem addressed in this paper is the identification of a model that accurately captures the flexible dynamic behavior of both the performance surface and the backplate, while having a limited number of available sensors, i.e., the total number of sensors for the performance surface and the backplate, denoted as  $n_{\rm s,ps}$  and  $n_{\rm s,bp}$  respectively, is less than the total number of actuators, denoted as  $n_a$ .

However, the number of sensors available does not directly provide access to an extensive backplate analysis. To overcome this limitation, an approach is developed that creates fictitious sensor readings. This is achieved by exploiting the large number of spatially distributed actuators to estimate the relative motion of the performance surface with respect to the backplate. Specifically, fictitious sensor readings are defined as the relative displacement between the performance surface and the backplate for all actuators located at the vector of positions  $\rho_{\rm a}.$  This can be mathematically expressed as

$$\bar{u}_{\text{a,rel}}(t) = \begin{bmatrix} u_{\text{ps}}(\rho_{\text{s,ps,1}}, t) - u_{\text{bp}}(\rho_{\text{s,bp,1}}, t) \\ \vdots \\ u_{\text{ps}}(\rho_{\text{s,ps,n_{\text{s,ps}}}}, t) - u_{\text{bp}}(\rho_{\text{s,bp,n_{\text{s,bp}}}}, t) \end{bmatrix}.$$
(10)

#### 2.4. Approach

The identification procedure is tailored to overactuated systems with a limited number of sensors, which includes deformable mirrors. The procedure includes the following steps:

- Frequency response function estimation. The first step is to estimate
  the FRFs of the system. The key step is the use of the local
  rational method, which is a local modeling method that is able
  to accurately estimate the FRFs of systems with a limited amount
  of data.
- 2. Modal model identification. The second step is to identify the modal model of the system. This is done using the FRFs that were estimated in the first step. The modal model is a mathematical representation of the system's dynamics, and it can be used for a variety of purposes, such as control design and structural analysis.
- 3. Fictitious sensors for overactuated systems. The third step is to add fictitious sensors to the system. Fictitious sensors are virtual sensors that are not physically present in the system, but they can be used to improve the spatial resolution of the modal model. The fictitious sensors are added to the system in such a way that they capture the relative dynamics of the backplate in (10), which is the structure that supports the deformable mirror.

The identification procedure described above is shown to powerful a tool for the analysis and control of overactuated systems with a limited number of sensors. The local rational method allows for short experiment time and accurate estimates, the modal model identification allows for modal models that are interpretable and may be used for control, and the fictitious sensors allow for the analysis of the underlying backplate dynamics that can be used to validate the structural design. The proposed techniques are demonstrated on a deformable mirror system.

#### 3. Frequency response function estimation

Frequency response measurements are an important first step for identifying the flexible dynamics of overactuated mechatronic systems. In this section, the approach for frequency response measurements of overactuated mechatronic systems is presented. In particular, the local rational method is introduced. This section constitutes Contribution C1.

#### 3.1. Local rational method

Consider the discrete signal u(n), n = 0, 1, ..., N - 1. The Discrete Fourier Transform (DFT) of u(n) is defined as

$$U(k) = \frac{1}{\sqrt{N}} \sum_{n=0}^{N-1} u(n) \exp\left(\frac{-i2\pi kn}{N}\right)$$
 (11)

where k denotes the kth DFT bin. Consider the linear-time-invariant system in Fig. 4 where u(n) denotes the input signal, y(n) denotes the output signal, and v(n) denotes the output noise. The output noise v(n) is colored noise in the sense that  $v(n) = H(\xi_k)e(n)$  where  $H(\xi_k)$  is the noise model and e(n) is zero-mean Gaussian white noise. The response of the system in Fig. 4 with respect to the discrete input u(n) in frequency domain equals

$$Y(k) = G_o(\xi_k)U(k) + T(\xi_k) + V(k)$$
(12)

where the transient response is denoted by  $T(\xi_k)$  and the output noise contribution at the kth frequency bin is denoted by V(k). The variable  $\xi_k$  denotes the frequency variable evaluated at DFT-bin k, which becomes  $\xi_k = j\omega_k$  in the Laplace domain and  $\xi_k = e^{j\omega_k}$  in the Z-domain.

The key mechanism of local modeling approaches is to exploit the local smoothness of the system by identifying a local model that is valid only over a small finite frequency range. This model can be used to provide a non-parametric estimate of  $G_o$  and the transient at the central DFT-bin k. To achieve this, a finite frequency window around DFT-bin k is considered, denoted by the variable  $r \in \mathbb{Z}$ , which can range from  $-N_W$  to  $N_W$ , i.e.

$$Y(k+r) = \tilde{G}_{k}(\xi_{k+r})U(k+r) + \tilde{T}_{k}(\xi_{k+r}) + V(k)$$
(13)

where  $\tilde{G}_k(\xi_{k+r})$  and  $\tilde{T}_k(\xi_{k+r})$  denote the kth local model of the system and the corresponding transients respectively. The parameter  $N_W$  allows to adjust the finite-frequency range on which the local parametric models are identified which is determined by the control engineer.

The open-loop setting in (12) is used to determine the frequency response results throughout this paper since the main application, i.e. a deformable mirror system, is open-loop stable. It is emphasized that the open-loop local rational modeling approach in (13) extends the closed-loop case, see e.g., [30].

#### 3.2. Parameterization & algorithm

The local models  $\tilde{G}_k(\xi_{k+r})$  are parameterized as local rational functions

$$\tilde{G}_k(\xi_{k+r}) = D_k^{-1}(r,\theta)N_k(r,\theta),\tag{14}$$

$$\tilde{T}_k(\xi_{k+r}) = D_k^{-1}(r,\theta)M_k(r,\theta),\tag{15}$$

where  $D_k(r) \in \mathbb{C}^{n_y \times n_y}$ ,  $N_k(r) \in \mathbb{C}^{n_y \times n_u}$ ,  $M_k(r) \in \mathbb{C}^{n_y \times 1}$  and  $\theta$  denote the common denominator matrix, system numerator matrix, the transient numerator vector, and parameter vector respectively

$$D_k(r,\theta) = I + \sum_{s=1}^{N_D} D_s(k,\theta) r^s,$$
 (16)

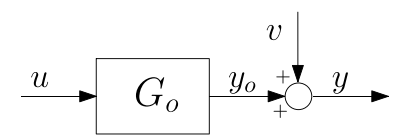


**Fig. 4.** Open-loop setting of a linear time invariant system with input u, measurement noise v, and output v.

$$N_k(r,\theta) = \sum_{s=0}^{N_N} N_s(k,\theta) r^s,$$
(17)

$$M_k(r,\theta) = \sum_{s=0}^{N_M} M_s(k,\theta) r^s.$$
 (18)

The order of  $D_k(r)$ ,  $N_k(r)$  and  $M_k(r)$  is denoted by  $N_D$ ,  $N_N$  and  $N_M$  respectively, see [31] for a detailed overview of parameterizations. The full polynomial parameterization form is considered in this paper as it encompasses a sufficiently rich class of systems with a limited number of parameters. This enables the selection of a small frequency window parameter  $N_W$  while maintaining a sufficient degree of averaging. The parameterization includes the local polynomial method case by selecting  $N_D=0$ . The model parameters in (16), (17) and (18) can be determined through dedicated algorithms [31].

The multivariable LRM is determined by solving the following linear least-squares problem for all k

$$\hat{\theta}(k) = \arg\min_{\theta} \sum_{r=-N_W}^{N_W} \left\| D_k(r,\theta) Y(k+r) - N_k(r,\theta) U(k+r) - M_k(r,\theta) \right\|_2^2.$$

$$(19)$$

The optimization method, which resembles the Levy method, is computationally efficient and accurate [31,46]. The possible estimation bias can be removed by invoking an iterative version of (19) which introduces an additional computational cost with typically limited improvement in estimation quality [31].

### 4. Identification and fictitious sensors of overactuated mechatronic systems

In this section, a unified approach is developed for identifying and analyzing modal models of mechatronic systems with a large number of spatially distributed actuators. First, a unified approach is developed for identifying modal models. Second, a method for creating fictitious sensors and conditions for creating fictitious sensors are presented. This section constitutes Contribution C2.

#### 4.1. Modeling overactuated mechatronic systems

The spatio-temporal behavior is defined by partial differential equations which are typically formulated using space–time-separated basis functions [41,47]

$$\begin{bmatrix} u_{\rm ps}(\rho, t) \\ u_{\rm bp}(\rho, t) \end{bmatrix} = \sum_{k=1}^{n_m} w_k(\rho) q_k(t). \tag{20}$$

The temporal contribution is determined by the generalized coordinates  $q_k(t)$  and the spatial contribution is determined by the vector  $w_k(\rho)$ . The number of basis functions is determined by the parameter  $n_m$ . Analytical solutions are not available in general and only exist for specific cases. For this reason, the solution often is limited to the nodal description of finite element method-based models that use a finite set of points in space.

Measurements are obtained based on  $n_a$  spatially distributed actuators. Since the actuators are connected to two surfaces, i.e., the backplate and the performance surface, a total of  $2n_a$  nodes are considered. Specifically, given the separation of space and time (20), the dynamics

can be formulated in the nodal coordinates  $q(t) = \begin{bmatrix} q_{ps}^{\mathsf{T}}(t) & q_{bp}^{\mathsf{T}}(t) \end{bmatrix}^{\mathsf{T}}$  that contain the nodes of the performance surface  $q_{ps}(t)$  and the backplate  $q_{bp}(t)$  at the vector of actuator locations  $\rho_a$ . This leads to a coupled set of second-order ordinary differential equations

$$M\ddot{q} + D\dot{q} + Kq = Qf(t) \tag{21}$$

where the mass matrix  $M \in \mathbb{R}^{2n_a \times 2n_a}$  is positive definite,  $D \in \mathbb{R}^{2n_a \times 2n_a}$  denotes the damping matrix,  $K \in \mathbb{R}^{2n_a \times 2n_a}$  denotes the stiffness matrix,  $Q \in \mathbb{R}^{2n_a \times n_a}$  denotes the input matrix, and  $f(t) \in \mathbb{R}^{n_a}$  denotes the input function at actuation locations  $\rho_a$ . Since the actuators are located between the performance surface and the backplate, the input matrix is partitioned as  $Q = \begin{bmatrix} I & -I \end{bmatrix}^\top$ .

The modal parameters are obtained by solving the undamped generalized eigenvalue problem

$$\left[K - \omega_k^2 M\right] \bar{\phi}_k = 0. \tag{22}$$

The eigenvalues,  $\omega_k^2$ , are the squared undamped eigenfrequencies and the eigenvector  $\bar{\phi}_k$ , which describes the kth mode shape vector, denotes the combination of the kth performance surface and backplate mode shape

$$\bar{\phi}_k = \left[\bar{\phi}_{\text{ns},k}(\rho_a)^{\mathsf{T}}, \bar{\phi}_{\text{bn},k}(\rho_a)^{\mathsf{T}}\right]^{\mathsf{T}} \tag{23}$$

where the mode shape  $\bar{\phi}_k$  is mass normalized, i.e.

$$\bar{\phi}_k^{\mathsf{T}} M \bar{\phi}_k = 1. \tag{24}$$

Throughout this paper, the scalar function  $\phi_{\mathrm{ps},k}(\rho): S_{\mathrm{ps}} \mapsto \mathbb{R}$  and  $\phi_{\mathrm{bp},k}(\rho): S_{\mathrm{bp}} \mapsto \mathbb{R}$  are the kth mass-normalized mode shape functions of the performance surface and the backplate respectively, which depend on the spatial variable  $\rho$ . To improve conciseness of the results, these functions are vectorized as  $\bar{\phi}_{\mathrm{ps},k}(\rho_{\mathrm{a}})$  and  $\bar{\phi}_{\mathrm{bp},k}(\rho_{\mathrm{a}})$  by evaluating the scalar functions  $\phi_{\mathrm{ps},k}(\rho)$  and  $\phi_{\mathrm{bp},k}(\rho)$  at the individual elements of the vector of actuator positions  $\rho_{\mathrm{a}}$  that are defined in (3).

The coupled set of differential equations (21) can be decoupled by introducing the coordinate transformation to modal coordinates, i.e.,  $q=\Phi\eta$ , where  $\Phi=\left[\bar{\phi}_1,\ldots,\bar{\phi}_{n_{\rm m}}\right]$ . Substituting the coordinate transformation and left multiplying (21) with  $\Phi^{\rm T}$  leads to

$$I\ddot{\eta} + D_m \dot{\eta} + K_m \eta = \begin{bmatrix} \bar{\phi}_{\mathrm{ps},1}(\rho_{\mathrm{a}})^{\mathsf{T}} \\ \vdots \\ \bar{\phi}_{\mathrm{ps},n_m}(\rho_{\mathrm{a}})^{\mathsf{T}} \end{bmatrix} - \begin{bmatrix} \bar{\phi}_{\mathrm{bp},1}(\rho_{\mathrm{a}})^{\mathsf{T}} \\ \vdots \\ \bar{\phi}_{\mathrm{bp},n_m}(\rho_{\mathrm{a}})^{\mathsf{T}} \end{bmatrix} f(t), \tag{25}$$

$$\begin{bmatrix} u_{\rm ps}(\rho,t) \\ u_{\rm bp}(\rho,t) \end{bmatrix} = \sum_{k=1}^{n_m} \begin{bmatrix} \phi_{\rm ps,k}(\rho) \\ \phi_{\rm bp,k}(\rho) \end{bmatrix} \eta_k(t) \tag{26}$$

where  $D_m = \Phi^T D \Phi = \operatorname{diag} \left( d_{m,1}, \ldots, d_{m,n_{\mathrm{m}}} \right)$ ,  $K_m = \Phi^T K \Phi = \operatorname{diag} \left( \omega_1^2, \ldots, \omega_{n_{\mathrm{m}}}^2 \right)$ , and  $\eta_k(t)$  are the modal coordinates. The deformation function (26) shows that the system is position dependent through the mode shape functions. Here, modal damping is considered which leads to the decoupled set of differential equations (25) and which is known to be representative of many lightly-damped systems in practice. Notice that due to the relative actuation, the input vector distributes the forces through a relative mode shape matrix in (25) that describes the mode shape of the performance surface with respect to the backplate.

#### 4.2. Identifying modal models

To identify the deformable mirror, measurement data is obtained at a finite number of spatially distributed sensors. Specifically,  $n_{\rm ps}$  sensors on the performance surface which locations are defined in the vector  $\rho_{\rm s,ps}$  and  $n_{\rm s,bp}$  sensors that measure the position of the backplate which locations are defined by the vector  $\rho_{\rm s,bp}$ . Consequently, instead of the position-dependent function in (26), a spatially sampled system is measured

$$\begin{bmatrix} \bar{u}_{ps}(t) \\ \bar{u}_{bp}(t) \end{bmatrix} = \sum_{k=1}^{n_m} \begin{bmatrix} \bar{\phi}_{ps,k}(\rho_{s,ps}) \\ \bar{\phi}_{bp,k}(\rho_{s,bp}) \end{bmatrix} \eta_k(t). \tag{27}$$

To improve the conciseness of the results, the deformation functions are vectorized as  $\bar{u}_{ps}(t)$  and  $\bar{u}_{bp}(t)$  by evaluating the scalar position-dependent deformation functions  $u_{ps}(\rho,t)$  and  $u_{bp}(\rho,t)$  at the individual elements of the vector of actuator positions  $\rho_{s,ps}$  and  $\rho_{s,bp}$ , which are defined in (6) and (9), respectively.

The application of the modal expansion theorem allows the reformulation of the system of equations in (25) and (27) to a summation of modal contributions

$$G(s) \in \mathbb{R}^{(n_{s,ps} + n_{s,bp}) \times n_a} : F(s) \mapsto U(s)$$
(28)

$$G(s) = \sum_{k=1}^{n_m} \frac{R_k}{s^2 + d_{m,k}s + \omega_k^2}$$
 (29)

where  $R_k$  denotes the rank-one modal participation matrix that is based on the sampled mode shape vectors and that is defined as

$$R_k = \begin{bmatrix} v_{\text{ps},k} \\ v_{\text{bo},k} \end{bmatrix} w_k^{\mathsf{T}} \tag{30}$$

$$\begin{bmatrix} v_{\mathrm{ps},k} \\ v_{\mathrm{bp},k} \end{bmatrix} = \begin{bmatrix} \bar{\phi}_{\mathrm{ps},k}(\rho_{\mathrm{s,ps}}) \\ \bar{\phi}_{\mathrm{bp},k}(\rho_{\mathrm{s,bp}}) \end{bmatrix} \qquad w_k = \left[ \bar{\phi}_{\mathrm{ps},k}(\rho_{\mathrm{a}}) - \bar{\phi}_{\mathrm{bp},k}(\rho_{\mathrm{a}}) \right]. \tag{31}$$

The modal participation matrix gives access to both a relative and absolute mode shape.

The aim is to identify a parametric modal model  $\hat{G}(\theta, s)$  which is defined by the modal form in (29). The parameterization is fully defined by the parameter vector

$$\theta = \operatorname{vec}\left\{\bar{d}_{m}, \bar{\omega}_{m}, R_{1}, \dots, R_{n_{m}}\right\}. \tag{32}$$

Here, the eigenfrequencies, the damping constants, and the modal participation matrices are denoted as  $\bar{\omega}_m = \left[\omega_{m,1},\ldots,\omega_{m,n_m}\right], \ \bar{d}_m = \left[d_{m,1},\ldots,d_{m,n_m}\right],$  and  $R_1,\ldots,R_{n_m}$  respectively.

The global parameters consisting of the damping ratio  $d_{m,i}$  and the resonance frequency  $\omega_k$  are estimated first. The parameters are estimated by estimating locally a second-order model to the elements of the frequency response estimate that is optimal in the least-squares sense. The values are averaged to obtain an accurate estimate of the global system parameters.

The second step involves the estimation of the modal participation matrix  $R_k$  in (35). Noting that at the resonance frequency, the response of (29) is approximately

$$G(j\omega_k) \approx \frac{-j\,R_k}{d_{m\,k}\omega_k}.$$
 (33)

Based on the frequency response estimate and the estimate of the global system parameters, the modal participation matrix is estimated, i.e.,

$$\tilde{R}_k \approx d_{m,k} \omega_k \Im \left\{ G(j\omega_k) \right\}. \tag{34}$$

This peak-picking method generally works well in practice [41]. The rank-one property of the modal participation matrix is enforced from the singular value decomposition, i.e.,  $\tilde{R}_k = U_k \Sigma_k V_{\nu}^{\mathsf{T}}$ , such that

$$R_k = \left[U_k\right]^1 \left[\Sigma_k\right]_1^1 \left[V_k\right]^{1^{\mathsf{T}}}.\tag{35}$$

The *i*th column and the *j*th row of the matrix, e.g.,  $V_k$ , are denoted by  $\left[V_k\right]^i$  and  $\left[V_k\right]_j$ , respectively. The method described by (34) generally works well with a sufficiently high resolution of the frequency response estimate. The obtained local parametric models can be interpolated, see e.g., [48], to improve the estimate of the modal participation matrix. Alternatively, an optimization-based approach can be pursued which could further improve the estimation [29,49].

#### 4.3. Fictitious sensors for analysis of overactuated mechatronic systems

A crucial step for the analysis of the modal model is the conversion of the modal participation matrix to a set of absolute and relative mass-normalized mode shape vectors in (30).

An important observation is that every rank-one matrix can be converted to a dyadic product of two vectors. **Theorem 1.** If  $R_k \in \mathbb{R}^{(n_{s,p_k}+n_{s,b_p}) \times n_a}$  is a rank-one matrix, then  $R_k$  can be decomposed into

$$R_k = \begin{bmatrix} \tilde{v}_{\text{ps},k} \\ \tilde{v}_{\text{bp},k} \end{bmatrix} \tilde{w}_k^{\mathsf{T}},\tag{36}$$

with  $\tilde{v}_{\text{ps},k} \in \mathbb{R}^{n_{\text{s,ps}}}$ ,  $\tilde{v}_{\text{bp},k} \in \mathbb{R}^{n_{\text{s,bp}}}$  and  $\tilde{w}_k \in \mathbb{R}^{n_{\text{a}}}$ .

**Proof.** The proof follows from the definition of the matrix rank, see e.g., [50, Section 3.115] and [51, Section 3.6].

Thus, every modal participation matrix, e.g., (35), is decomposed into a product of mode shape vectors. The key issue is that the decomposition is non-unique. For instance  $\left[\alpha \tilde{v}_{\mathrm{ps},k}^{\mathsf{T}}, \alpha \tilde{v}_{\mathrm{bp},k}^{\mathsf{T}}\right]^{\mathsf{T}} \frac{1}{a} \tilde{w}_{k}^{\mathsf{T}}$  with any nonzero  $\alpha \in \mathbb{R}$  is a solution. Thus, the mode shape vector is unique up to a scaling constant [52]. The following result provides a sufficient design requirement for finding a unique decomposition of the modal participation matrix into mass-normalized mode shape vectors.

**Theorem 2.** Let  $R_k$  be a rank-one modal participation matrix of a system according to (28) with  $n_a$  actuators,  $n_{ps,a}$  sensors on the performance surface, and  $n_{bp,a}$  sensors on the backplate. If there exists at least one collocated sensor-actuator triplet, i.e.,  $\rho_{s,ps,i} = \rho_{s,bp,j} = \rho_{a,k}$  with  $i,j,k \in \mathbb{N}$ , then the decomposition in (31) can be uniquely determined.

A proof of Theorem 2 is provided in Appendix. Essentially, Theorem 2 enables the extraction of mass-normalized mode shape vectors by a design requirement, i.e., at least one collocated sensor-actuator triplet should be present. The triplet must consist of a sensor on the backplate, a sensor on the reflective surface, and an actuator that are all collocated. This enables a qualitative comparison of both the relative and absolute mode shape vectors.

The key drawback of conventional modeling techniques is that these techniques fully rely on the sensor data. The key idea in this paper is that in the modal description, e.g. Eq. (29), the mode shape vectors are encountered twice. Specifically, the mode shape vector is sampled at the sensor and actuator locations. To enhance the physical insight into deformable mirror systems, the relative mode shape vector sampled by actuators is employed. This provides additional information about the relative system dynamics, i.e., the behavior of the performance surface with respect to the backplate. Moreover, since deformable mirrors are equipped with a large number of spatially distributed actuators, the spatial density of the modal description is increased significantly. The relative system dynamics are estimated as

$$\hat{G}_{\text{rel}}(s) = \sum_{k=1}^{n_m} \frac{R_{\text{rel},k}}{s^2 + d_{m,k}s + \omega_k^2},\tag{37}$$

$$R_{\text{rel},k} = \tilde{w}_k \tilde{w}_k^{\mathsf{T}}. \tag{38}$$

Interestingly, (37) provides the fictitious sensors in (10) and enables to analyze the relative system behavior without having sensors that measure the relative system dynamics. Interchanging the role of sensors and actuators underlying Theorem 2 is known as the Betti–Maxwell theorem, see e.g., [39,40,42].

#### 5. Simulation case study

In this section, a simple simulation case study is discussed which intends to illustrate the unified approach presented in Sections 3.1 and 4. The case study encompasses all steps from frequency response function identification to the formulation of a modal model and the prediction of fictitious sensors. The system description and the aim of the case study are discussed first. Second, the unified approach presented in Sections 3.1 and 4 is executed. Lastly, the quality of the obtained results is analyzed. This section constitutes Contribution C3.

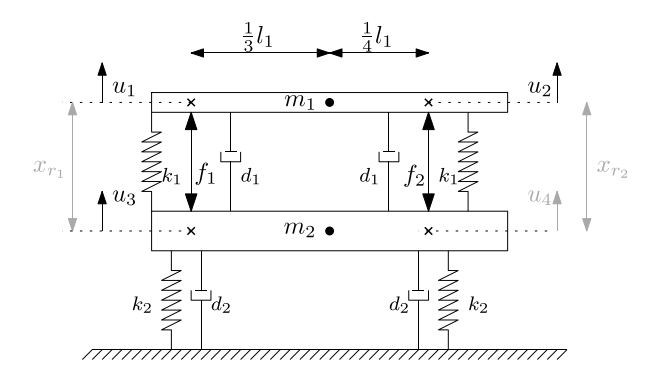


**Fig. 5.** Freebody diagram of the system considered in the simulation case study. The system is a rigid-body approximation of a deformable mirror. The performance surface and the backplate have a mass  $m_1$  and  $m_2$  respectively. The system is equipped with two actuators  $f_1$  and  $f_2$ , two sensors  $u_1$  and  $u_2$  on the performance surface and one sensor on the backplate  $u_3$ . The aim of the case study is to predict the behavior of the fictitious sensors  $u_r$ , and  $u_4$ .

#### 5.1. System description & aim

The free body diagram of the system considered in the simulation case study is depicted in Fig. 5. The system is a rigid-body simplification of the one-dimensional deformable mirror representation in Fig. 3. In this model, the backplate  $m_2$  is heavy in relation to the performance surface  $m_2$  and therefore  $m_2 > m_1$ . The actuators deform the mirror but have only a marginal effect on the support structure, hence,  $k_2 > k_1$ . It is emphasized that in this simulation the performance surface and backplate are modeled as rigid bodies. Hence, the system can be described by four degrees of freedom, representing the translation and rotation of each body.

The system considered in the simulation case study is equipped with two actuators that are positioned between the two rigid bodies, i.e. relative actuation. To illustrate the effectiveness of the proposed approach, a setting with limited sensing capabilities is created. Specifically, two position sensors measure the position of the performance surface, and only one sensor measures the displacement of the backplate. The backplate sensor  $u_3$  is collocated with the actuator  $f_1$  and performance surface sensor  $u_1$ . The aim of the case study is to predict the behavior of the unmeasured sensor  $u_4$  through the fictitious sensor output  $u_{r_2}$  using the tools presented in the paper.

#### 5.2. Procedure

The aim of this section is to identify the full system behavior

$$G_{\rm f} = \left[ \begin{array}{c|c} G_{\rm ps}^* & G_{\rm bp}^* \end{array} \right]^* \tag{39}$$

$$= \begin{bmatrix} f_1 & f_2 \end{bmatrix}^{\mathsf{T}} \mapsto \begin{bmatrix} u_1 & u_2 \mid u_3 & u_4 \end{bmatrix}^{\mathsf{T}}$$

$$(40)$$

while having access to a subsystem with three sensors, i.e.

$$G_{\rm s} = \left[ \begin{array}{c|c} G_{\rm ps}^* & G_{\rm bp,s}^* \end{array} \right]^* \tag{41}$$

$$= \begin{bmatrix} f_1 & f_2 \end{bmatrix}^\mathsf{T} \mapsto \begin{bmatrix} u_1 & u_2 \mid u_3 \end{bmatrix}^\mathsf{T} \tag{42}$$

This is achieved by applying the method proposed in Section 4. In particular, this is achieved by first estimating the relative system behavior through the fictitious sensors in (37). Based on the relative system behavior, the full response in (39) is recovered.

#### 5.2.1. Step 1: Frequency response measurement

The frequency domain-based procedure presented in Section 3.1 is pursued to identify a non-parametric model of  $G_{\rm S}$  Since the system is stable, open-loop experiments are performed. Two white Gaussian noise signals are injected into the inputs. The identified element-wise Bode magnitude plot of the resulting frequency response function estimate of the  $G_{\rm S}$  and the true full system  $G_{\rm f}$  is depicted in Fig. 7.

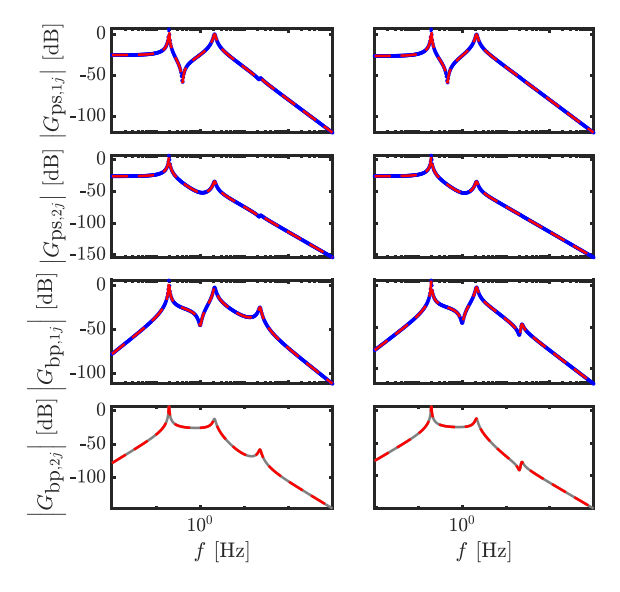


**Fig. 6.** Element-wise Bode magnitude plot of the true system  $G_{\mathbf{f}}$  (••••), the parametric modal model of the subsystem  $\hat{G}_{\mathbf{f}}$  (••••), and estimated full system  $\hat{G}_{\mathbf{f}}$  (••••). It is emphasized that  $\hat{G}_{\mathbf{f}}$  is estimated using the non-parametric estimate of the subsystem  $G_{\mathbf{s}}$  only and the full system  $G_{\mathbf{f}}$  is only visualized for validation purposes. Thus, the behavior at  $u_{\mathbf{t}}$  is estimated through the use of a fictitious sensor introduced in Section 4.3.

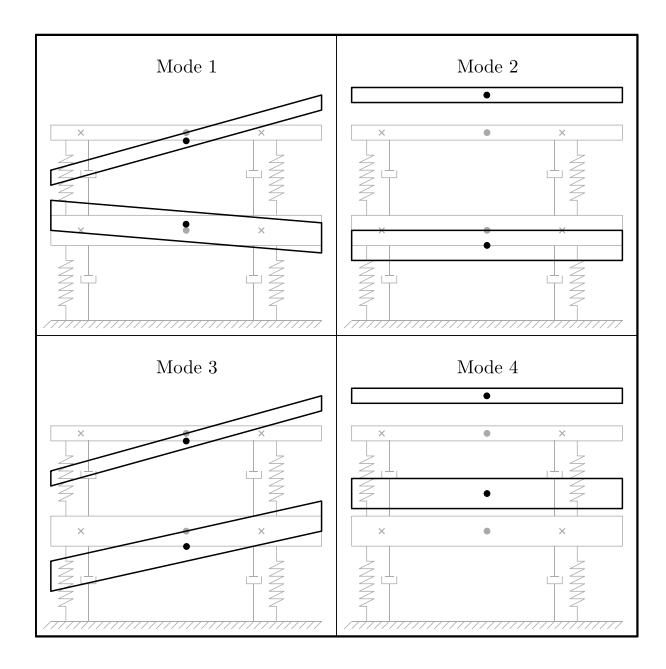


**Fig. 7.** Schematic overview of the four modes of the system, i.e., the two rotational modes, and two translational modes. These modes are based on the modal model of the full system  $G_{\rm f}$ . It is emphasized that the full modal behavior of the system is recovered through the use of fictitious sensors introduced in Section 4.3.

#### 5.2.2. Step 2: Modal model identification

This subsection aims to identify a parametric modal model of  $G_{\rm s}.$  Modal models are estimated of the form

$$\hat{G}_{s} = \left[ \begin{array}{c|c} \hat{G}_{ps}^{*} & \hat{G}_{bp,s}^{*} \end{array} \right]^{*} \tag{43}$$

$$= \sum_{k=1}^{4} \frac{\hat{R}_k}{s^2 + d_{m,k} s + \omega_k^2}.$$
 (44)

Since the system has four degrees of freedom, four modes are considered. To identify the modal model in Eq. (43), the algorithm introduced

in Section 4 is applied. The element-wise Bode magnitude plot of the modal model is depicted in Fig. 6. The Bode plot reveals that the modal model accurately fits the frequency response measurement. However, the analysis of the modal model in the current form, (43), provides limited information about the dynamic behavior of the backplate.

#### 5.2.3. Step 3: Fictitious sensors: Relative system behavior

The key step in the reconstruction of the full system  $G_{\rm f}$  using the modal model of the subsystem  $G_{\rm s}$  is to estimate the relative system behavior through the fictitious sensors that are introduced in Section 4.3.

The first sensor  $u_1$  is collocated with actuator  $f_1$  and sensor  $u_3$ . Consequently, Theorem 2 holds and the modal participation matrix  $R_k$  in (43) is uniquely decomposed into mass-normalized mode shape vectors

$$R_k = \begin{bmatrix} \tilde{v}_{\text{ps},k} \\ \tilde{v}_{\text{bp},k} \end{bmatrix} \tilde{w}_k^{\mathsf{T}},\tag{45}$$

with  $\tilde{v}_{\mathrm{ps},k} \in \mathbb{R}^2$ ,  $\tilde{v}_{\mathrm{bp},k} \in \mathbb{R}^1$  and  $\tilde{w}_k \in \mathbb{R}^2$ . The relative system behavior is estimated by exploiting the relative mode shape vector  $\tilde{w}_k$ 

$$\hat{G}_{\text{rel}} = \hat{G}_{\text{bp}} - \hat{G}_{\text{ps}} \tag{46}$$

$$= \sum_{k=1}^{4} \tilde{w}_k \frac{1}{s^2 + d_{mk} s + w_k^2} \tilde{w}_k^{\mathsf{T}}. \tag{47}$$

Essentially,  $\hat{G}_r$  describes the displacement of the performance surface with respect to the backplate. The full system behavior of the backplate is recovered by combining the relative system behavior in (46) with the absolute system behavior of the performance surface in (43), i.e.,

$$\hat{G}_{bp} = \hat{G}_{ps} + \hat{G}_{rel} \tag{48}$$

Combining the modal model of the backplate in (48) with the identified modal model of the performance surface in (43) leads to the modal model of the full system

$$\hat{G}_{f} = \left[ \begin{array}{c|c} \hat{G}_{ps}^{*} & \hat{G}_{bp}^{*} \end{array} \right]^{*} \tag{49}$$

The resulting element-wise Bode magnitude plot is depicted in Fig. 6.

#### 5.3. Results

When analyzing the frequency response estimate of  $G_{\rm s}$  in Fig. 6, the analysis of the dynamic behavior of the backplate is limited to a temporal analysis in view of the physical sensors only. Consequently, the dynamic behavior of the backplate is unclear. In sharp contrast, the approach proposed in this paper allows identifying the full response  $G_{\rm f}$  by exploiting the modal framework. In particular, the approach allows analyzing the full behavior of the backplate through the application of fictitious sensors in (37). In addition, this method enables analyzing the modal behavior through visualization of the mode shape vectors in Fig. 7. It is emphasized that this example is a simplification of the deformable mirror and is intended to illustrate the advantage of the proposed approach.

#### 6. Experimental case study

In this section, the results so far are illustrated in an experimental case study. The case study includes a deformable mirror setup, see Fig. 8. The case study encompasses all steps from frequency response function identification to the formulation of a modal model and the analysis of mechanical modes. The experimental setup is explained first. Second, the frequency response estimation procedure is discussed. Third, fictitious sensors are constructed by exploiting the modal modeling framework. Lastly, the obtained results are analyzed by using the outputs of the fictitious sensors, and several design suggestions are provided. This section constitutes Contribution C4.

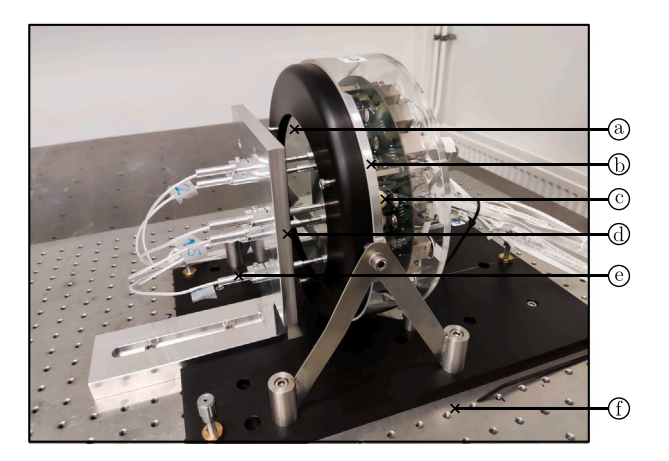


**Fig. 8.** Experimental test setup including the DM1 deformable mirror which is designed by TNO [10]. ⓐ performance surface, ⓑ backplate, ⓒ actuator, ⓓ sensor bracket, ⓔ capacitive sensor, and ⓓ testbench.

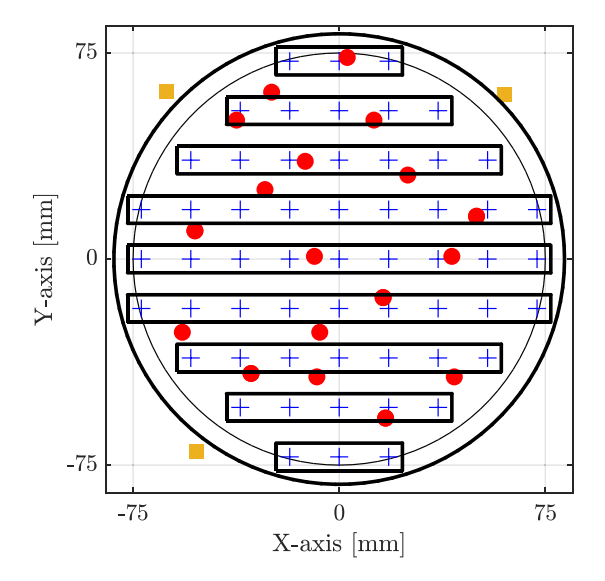


**Fig. 9.** Schematic top view of the deformable mirror setup indicating the positions of the actuators and sensors. The actuator locations  $\rho_{\rm a}$  (+ ) are connected to the performance surface and the backplate. The capacitive sensors (  $\blacksquare$ ) which are located at  $\rho_{\rm s,ps}$  measure the position of the performance surface, and the acceleration sensors (  $\blacksquare$ ) are connected to the backplate and are located at  $\rho_{\rm s,bo}$ .

#### 6.1. Setup

In this case study, a prototype deformable mirror system is used which is considered representative for future deformable mirrors. The prototype is depicted in Fig. 8. The prototype deformable mirror has a mirror diameter of 150 mm. The deformable mirror contains 52 operational actuators that enable the deformation of the performance surface. These actuators are connected to a backplate that is circular and has a specific inner geometry of milled parts, see Fig. 9.

A host/target computer setup is used to conduct the experiments. The host computer is a windows computer with Matlab/Simulink which is used to compile C-code which is forwarded to the target computer. The target computer runs on real-time Linux. Experiments are conducted with a sampling frequency of 4 kHz. The deformable mirror is has hybrid reluctance actuators, see [10] for details. The actuation signal is generated with a 16-bit DAC with 64 channels with dedicated amplifiers that are located on the back of the deformable mirror, see [10] for details. The deformation of the deformable mirror is measured with a temporary sensor setup consisting of six sensors that

are used to measure the deformation of the performance surface and three sensors that are connected to the actuator backplate. The sensors that measure the deformation of the performance surface are Lion Precision Capacitive Sensors C5 with CPL290 read out electronics with a 16-bit ADC and a resulting resolution of 3.8 nm. The sensors on the backplate are B&K 4508 accelerometers.

The setup is mounted on a rigid and heavy test bench, see Fig. 8. The capacitive sensors that measure the deformation of the performance surface are mounted to a movable aluminum bracket. The sensor bracket is relocated four times to enhance the spatial resolution in the analysis. For calibration and validation purposes, the sensor bracket is relocated such that there is some overlap in the resulting sensor locations. For this reason, the deformation of the performance surface is measured on 18 unique positions, see Fig. 9.

The measured positions are relative with respect to the aluminum bracket. These positions are assumed absolute due to the high stiffness of the bracket, the rigid and heavy test bench, and the bracket not being in the force loop. Also, three acceleration sensors are used to measure the absolute deformation of the backplate. The acceleration sensors are all non-collocated due to the limited available space, i.e., these acceleration sensors are positioned beyond the area covered by the performance surface. The experiments are conducted in an open-loop setting.

#### 6.2. Frequency response function estimation

In this section, the frequency response function of the experimental deformable mirror is estimated. The estimation is performed using the local rational method introduced in Section 3.1.

From the excitation signals, u, and the noisy outputs, y, the FRF of the system,  $G_o$ , is determined using the LRM introduced in Section 3.1. All inputs of the system are simultaneously excited by  $n_a=52$  independently generated Gaussian white noise signals with zero mean. The experiment time of a single experiment is 60 s.

The sensor bracket that measures the deformation of the performance surface is repositioned four times to enhance the spatial resolution of the position measurement. During the last measurement, five capacitive sensors covered the deformable mirror. Also, a separate measurement is performed to measure the response of the backplate with the three acceleration sensors. For this reason, five independent experiments are conducted, hence, LRM is used five times to construct the frequency response estimation. The resulting  $26 \times 52$  element-wise Bode magnitude plot is depicted in Fig. 10, and a subset is depicted in Fig. 11.

Interestingly, Figs. 10 and 11 reveal first-order roll-off at approximately 600 Hz in all elements of the Bode magnitude plot. This effect is caused by relatively high inductance compared to the resistance of the actuator. Also, the element-wise Bode magnitude plot in Fig. 10 indicates strong collocated and noncollocated behavior. The magnitude in the collated case is relatively large. In sharp contrast, the magnitude in the noncollocated case is generally low. However, at resonance frequencies, a high response can be recognized. This confirms that flexible dynamics lead to inherently multivariable system dynamics which confirms the importance of modeling the flexible dynamics for analysis and control. Also, the element-wise Bode plot reveals that design analysis and control design directly based on the frequency response measurement is practically unfeasible due to the large number of inputs and outputs and the complicated temporal nature of the dynamics. Therefore, the figure confirms the importance of the development of a unified approach for the identification models for mechanical design analysis and control design, which is the aim of this manuscript.

#### 6.3. Modal models

The aim of this section is to identify a modal model of the experimental deformable mirror based on the frequency response function estimate. First, the mechanical system behavior is isolated by preprocessing the data. Second, the modal model is estimated based on the method introduced in Section 4.

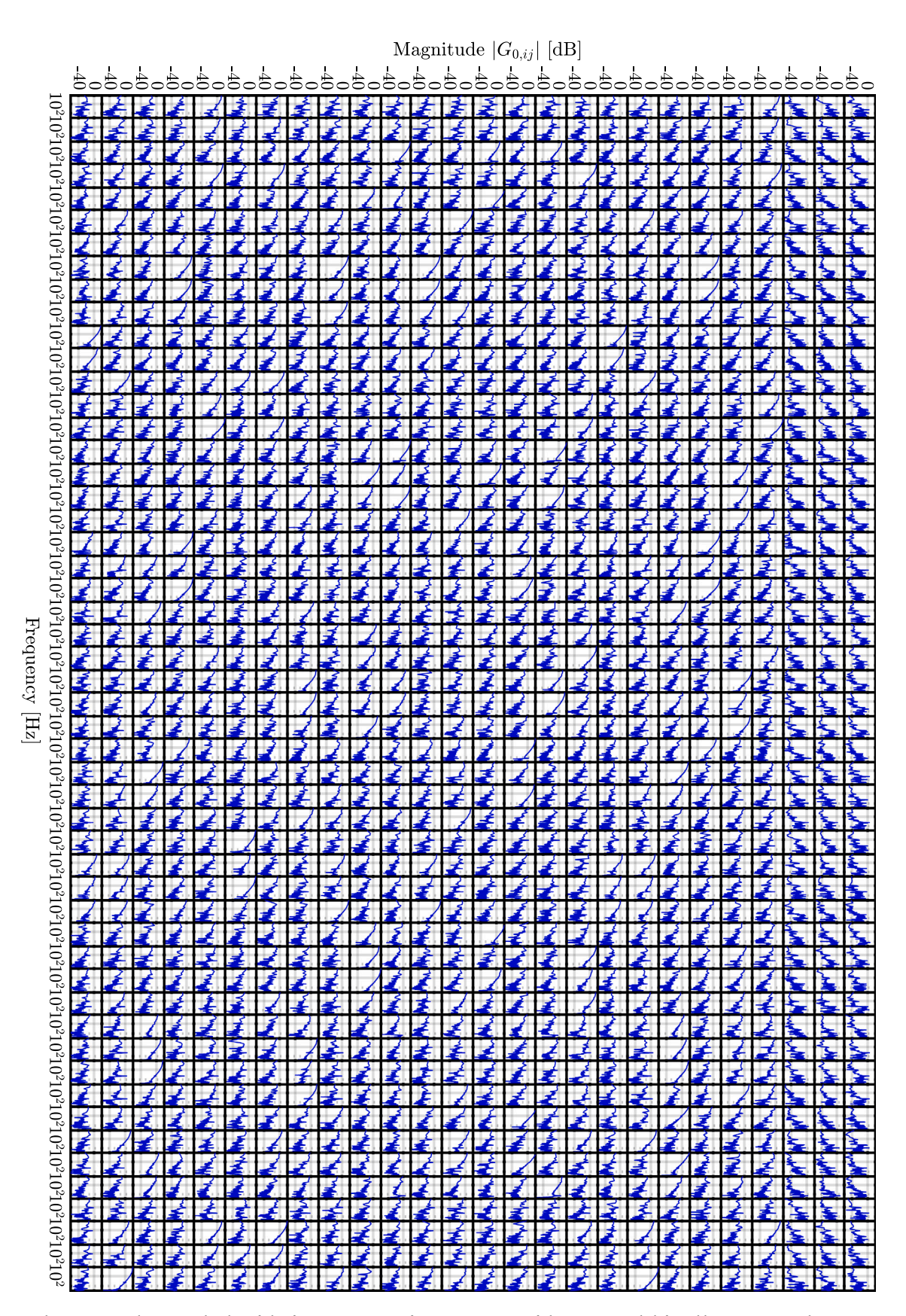


Fig. 10.  $26 \times 52$  element-wise Bode magnitude plot of the frequency response function estimation of the experimental deformable mirror DM1. The top 3 rows of the Bode magnitude plot represent the transfer to the acceleration sensors mounted to the backplate. The remaining rows represent the transfer to the capacitive sensors measuring the absolute displacement of the performance surface. The estimate is made using the local rational method introduced in Section 3.1 with five experiments of 60 s. The figure is depicted to highlight the high complexity of the system due to the large number of inputs and outputs and the high-order temporal behavior.

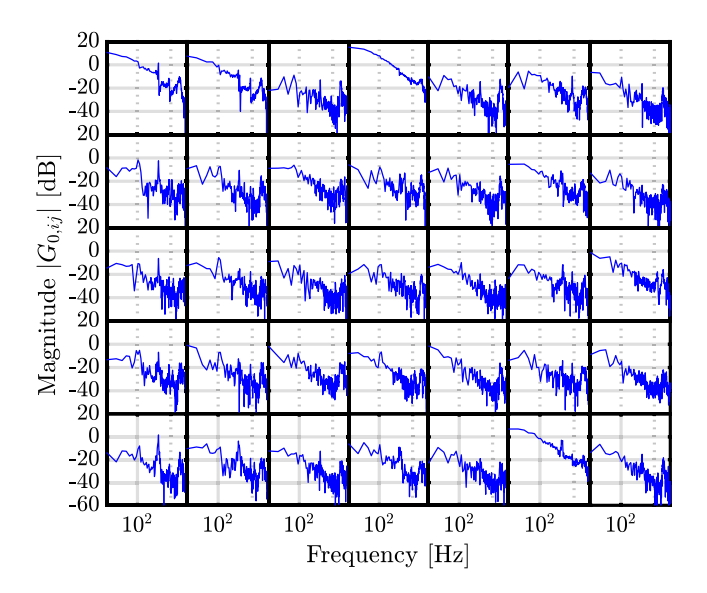


Fig. 11. Element-wise Bode magnitude plot of a  $5 \times 7$  subset of the frequency response estimation (  $\longrightarrow$  ) of the experimental deformable mirror DM1.

#### 6.3.1. Pre-processing

An important step to identifying a modal model is to isolate the modal systems dynamics. First, the acceleration sensor data is integrated twice to mimic position data. Second, the phase effect of the computational delay due to the input–output and zero-order hold delay is compensated for. Third, the frequency response function estimation also contains first-order dynamics of the actuators. The actuator roll-off may slightly vary between actuators due to manufacturing tolerances. For this reason, the first-order actuator roll-off is removed in a column-wise manner by identifying and subsequently compensating a first-order model of the form  $G_{\rm act} = \frac{1}{1+\frac{3}{\omega_c}}$ . The resulting pre-processed frequency response estimate is depicted in Fig. 12.

#### 6.3.2. Modal model identification

A modal model is estimated by the procedure described in Section 4. The first  $n_m = 11$  flexible modes are identified. A subset of the resulting modal model is depicted in Fig. 12.

The modal model is validated by comparing the frequency response to the experimental data in Fig. 12. First, it can be observed that the collocated system behavior is accurately identified. Second, the non-collocated sensor-actuator pairs indicate a generally low mechanical response compared to the noise floor. At the resonance frequencies, the modal model accurately matched the frequency response data. Overall, the modal model accurately describes the mechanical behavior of the deformable mirror. The large responses for both the collocated and noncollocated sensor-actuator pairs indicate that the flexible dynamic behavior leads to inherently multivariable behavior which must be accounted for in the control architecture. This means that the control system must be designed to take into account the coupling between the different actuators and sensors. This confirms the necessity of identifying the flexible dynamic system behavior of next-generation deformable mirrors.

#### 6.3.3. Fictitious sensors

In Section 4.3, the identified modal participation matrix is decomposed into mass-normalized mode shape vectors. These vectors describe the absolute modal behavior at the sensor locations and the relative system behavior at the actuator locations. However, the sensors on the backplate are positioned outside of the area covered by the performance surface, meaning that there is no collocated sensor-actuator triplet. As a consequence, Theorem 2, which enables to calculation

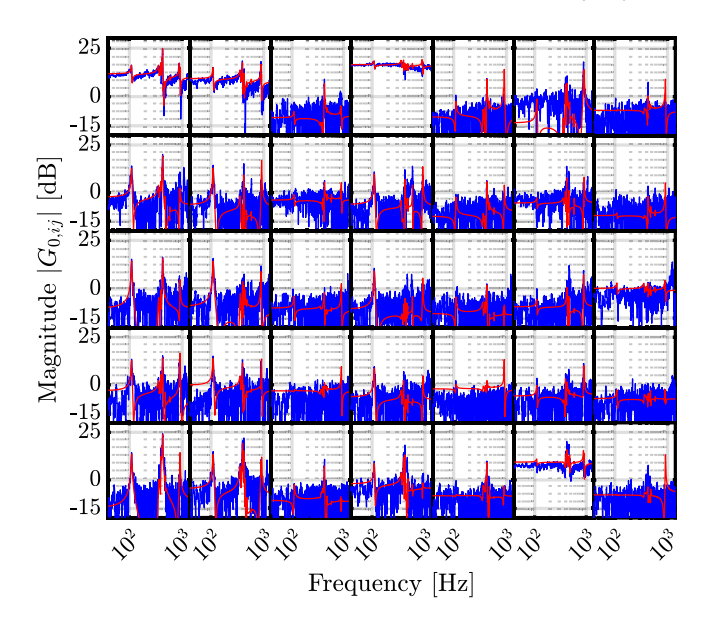


Fig. 12. Element-wise Bode magnitude plot of a  $5 \times 7$  subset of the frequency response estimation (  $\longrightarrow$  ) and the modal model (  $\longrightarrow$  ).

of mass-normalized mode shape vectors from the modal participation matrix, cannot be applied. However, the modal participation matrix can be decomposed into arbitrarily scaled mode shape vectors. These mode shape vectors can be analyzed to gain insight into the structural dynamics of the system, but they cannot be qualitatively compared or combined. This is because the scaling factors are arbitrary and cannot be determined from the data.

To obtain the mode shape vectors, the procedure in Section 4.2 is applied. For this reason, the mode shape vectors are normalized with respect to the largest singular value of the modal participation matrix. It is emphasized that although these mode shape vectors are not mass-normalized, these can still be useful for design analysis. In particular, the relative system behavior can still be analyzed without having relative sensors. Also, the number of actuators is large and thus the relative mode shape vectors may reveal detailed insights about the backplate and reflective surface system dynamics.

#### 6.3.4. Mode shape visualization

The mode shape vectors are interpolated to visualize and subsequently analyze the identified mechanical modes. A widely used interpolation method is the smoothed-thin-plate spline interpolation approach [53]. From a physical point of view, the thin-plate spline is based on minimizing the bending energy of a thin elastic plate. For this reason, the spline might be particularly suitable for modeling the deformation of the performance surface and the backplate as the out-of-plane dimensions are small compared to the in-plane dimensions.

Given a set of  $n_d$  coordinates  $(x_j, y_j) \in \mathbb{R}^2$  and  $n_d$  corresponding mode shape samples  $z_j \in \mathbb{R}$ . The smoothed thin-plate-spline interpolating spline  $\mathcal{W}_s$  is the unique optimum to the cost function

$$\min_{\mathcal{W}_s} \sum_{j=1}^{n_d} \left| \mathcal{W}_s(x_j, y_j) - z_j \right|^2 + \lambda U$$
 (50)

where

$$U = \int_{-\infty}^{\infty} \int_{-\infty}^{\infty} \Delta^2 \mathcal{W}_s(x, y) dx dy.$$
 (51)

The function U is generally interpreted as a measure of the bending energy of the spline function. The smoothing parameter  $\lambda$  provides a trade-off between robustness to estimation errors and interpolation accuracy. In this paper, the values of the smoothing parameters are determined using a Leave-One-Out-Cross-Validation (LOOCV) approach,

i.e., the value of  $\lambda$  is used which minimizes the LOOCV error [53]. This interpolation is carried out independently for each mode shape. It is emphasized that for each mode shape a different smoothing parameter  $\lambda$  is computed. The resulting mode shape visualizations are shown in Fig. 13.

#### 6.4. Mode shape analysis

As described in Section 4, the sensors of both the performance surface and the backplate are absolute. Hence, their corresponding mode shape vectors are absolute. In sharp contrast, the actuation is relative, hence, the corresponding mode shape vectors describe the mode shape of the performance surface with respect to the actuator backplate. Note that the analysis is based on the procedure in Section 4.3 that enables to analyze the relative system behavior without having sensors that measure the relative displacement.

1. The mode at 111 Hz in Fig. 13 reveals that the performance surface is barely moving compared to the backplate indicated by the acceleration sensors. The relative mode shape reveals a tipping motion indicating that the backplate is tipping around the *Y*-axis. As a consequence, from these mode shape vectors can be concluded that the mode at 111 Hz is dominated by a rigid-body motion of the backplate.

2. Between 400-600 Hz a significant number of modes can be

- observed in Fig. 12. One of these modes, e.g., at 463 Hz, is visualized in Fig. 13. Interestingly, the relative mode shape indicates complicated system dynamics that coincide with the location of the beam-based inner geometry of the backplate. Despite the limited number of sensor locations on the performance surface, the absolute mode shape of the performance surface reveals that the complicated deformation pattern seems to propagate to the performance surface, especially near the sensor locations. The complicated dynamics originates from the backplate design, i.e., the bending mode of the strips that support the actuators. Interestingly, the longest strips start resonating at approximately 400 Hz, and in the subsequent modes, the remaining shorter strips resonate. These modes complicate the control design as these are complex in the spatial sense, and there are a lot of these modes in a short frequency interval. Therefore, the information revealed by the proposed method could be used to improve the
- 3. The mode at 1826 Hz in Fig. 13 reveals a flexible mode of the performance surface. At this frequency, the relatively high mass of the support structure prevents the backplate from moving which is confirmed by the absolute mode shape of the backplate measured by the acceleration sensors. In sharp contrast, the mode shape of the performance surface reveals that it is severely vibrating. This is confirmed by the deformation pattern of the relative mode shape which coincides with the deformation pattern of the absolute performance surface mode shape.

mechanical design of the deformable mirror backplate such that

less complicated flexible dynamics are obtained.

#### 6.5. Discussion

The experimental case study demonstrates the effectiveness of the proposed tools from frequency response estimation to identifying modal models and analyzing the obtained results. The design analysis reveals flexible dynamics associated with the geometry of the backplate, which is complicated both in spatial and temporal sense. This could be taken into account in future backplate design such that less complicated flexible dynamics is obtained. Also, the sensors on the backplate are all located outside the area covered by the performance surface due to space limitations. Consequently, due to the lack of collocation, Theorem 2 is not valid and the mode shape vectors cannot be mass normalized. Future designs of deformable mirrors could benefit from at

least one location on the actuator backplate that enables the collocation of at least one backplate sensor with at least one actuator. This ensures that there is a collocated actuator–sensor triplet which is required in Theorem 2. This enables the modal participation matrix to be decomposed in mass-normalized mode shape vectors which would further enhance the analysis through qualitative comparison of the mode shape vectors and the creation of fictitious sensors.

In comparison to previous studies, the proposed approach offers several advantages. First, existing experimental methods in the literature that focus on deformable mirrors ignore the temporal system behavior and therefore focus on the static system behavior [7,19-21]. In contrast, this paper includes the spatio-temporal nature of the flexible dynamic behavior. Second, existing identification methods that do consider the spatio-temporal nature of the flexible dynamic behavior are typically based on simulations [22-26]. Compared to these studies, the approach in this paper offers limited user intervention since it does not rely on prior system knowledge and advanced modeling techniques. Third, compared to other modal model identification techniques, e.g., that consider a time domain-based parametric identification approach, the identification approach is frequency domain based which is data efficient and interpretable [38,41]. Fourth, compared to traditional frequency response estimation techniques methods such as spectral analysis, the local rational method which is used in this paper requires significantly less experiment time [10,27-29]. Also, in contrast to existing literature, the local rational method is used in an experimental case study with a large number of inputs and outputs. Fifth, compared to existing parametric modal model identification techniques, e.g., [29], the approach in this paper is relatively simple and therefore requires less user intervention. Sixth, the large number of spatially distributed actuators are used as fictitious sensors by exploiting the modal system description. Compared to conventional structural analysis approaches, this approach does not require an impact hammer [38,41].

These models are envisioned to be useful in preparation for controller design for deformable mirror systems. A modal decoupling strategy can be devised that specifically addresses the flexible dynamics that inherently challenge control efforts. In scenarios where explicit measurements of the flexible dynamics are unattainable, such as when the deformable mirror is integrated into a telescope and no explicit position measurements are available, the modal model could have a pivotal role. Through the modal model, the flexible dynamics can be estimated and subsequently addressed by control. Also, the obtained model provides a good starting point to address the spatio-temporal nature explicitly through inferential control techniques.

#### 7. Conclusions

This paper presents an identification approach that is tailored to design validation and control design of overactuated systems with a limited number of temporary position and acceleration sensors with limited experiment time and limited user intervention. Moreover, the models provide physical insights into the flexible dynamic behavior. The proposed unified approach encompasses the steps from the estimation of a frequency response function to the identification and analysis of through fictitious sensor. The case study illustrates the effectiveness of the proposed approach.

Compared to existing work, the method proposed in this paper does not rely on complicated FEM modeling techniques. Instead, an experiment-based approach is pursued. Additionally, the proposed method does not fully rely on the limited number of sensors that are available to analyze the system. Instead, the proposed method complements the limited number of sensors with fictitious sensor information, which employs the mode shape vectors of the actuators, of which a large number is present. The experimental case study demonstrates the effectiveness of the proposed approach and reveals a specific design consideration in the actuator backplate. This information could be

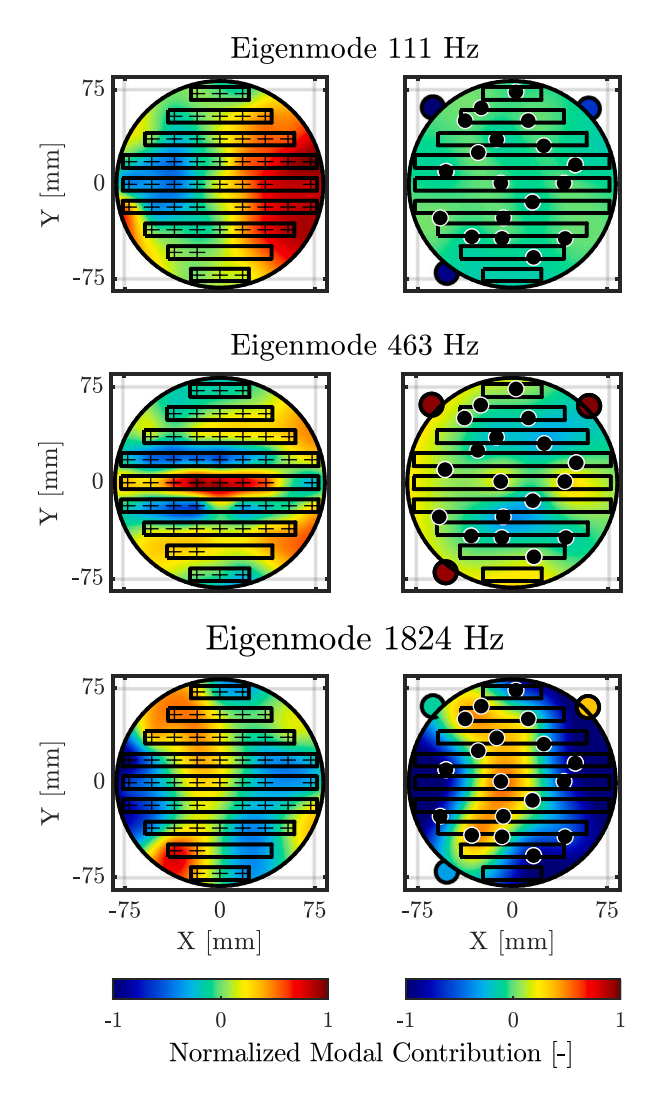


Fig. 13. Vizualization of three mechanical modes of the experimental deformable mirror system DM1. The left figures visualize the relative mode shape vectors from the actuator perspective. The actuators are indicated with a marker (+). The right figures visualize the absolute mode shape vectors from the sensor perspective. The capacitive sensors that measure the absolute displacement of the performance surface are indicated by ( ●) and the acceleration sensors ( O) measure the acceleration of the backplate. The modal contribution is indicated by the colormaps. Notice that the colormaps are normalized to one.

used to improve the design of deformable mirrors and to enhance the performance in adaptive optics for ground-based astronomy.

Summarizing, the proposed approach enables analysis through the visualization of flexible modes and subsequently acts as an enabler for next-generation motion control of adaptive secondary mirrors for ground-based astronomy. Current research focuses on using the obtained models for control techniques that specifically target the flexible dynamic behavior. Through the proposed approach, measurements could be obtained, the fictitious sensor could be useful for control by providing insight and estimates of the flexible dynamics. Also, the obtained models provide a starting point for inferential control.

#### CRediT authorship contribution statement

**Paul Tacx:** Conceptualization, Data curation, Formal analysis, Investigation, Methodology, Software, Validation, Visualization, Writing – original draft, Writing – review & editing, Funding acquisition, Project administration, Resources, Supervision. **Roel Habraken:** Conceptualization, Data curation, Formal analysis, Investigation, Methodology,

Visualization, Writing – original draft, Writing – review & editing, Funding acquisition, Project administration, Resources, Software, Supervision, Validation. Gert Witvoet: Conceptualization, Investigation, Methodology, Supervision, Validation, Writing – original draft, Writing – review & editing, Data curation, Formal analysis, Funding acquisition, Project administration, Resources, Software, Visualization. Marcel Heertjes: Conceptualization, Data curation, Formal analysis, Funding acquisition, Investigation, Methodology, Project administration, Resources, Software, Supervision, Validation, Visualization, Writing – original draft, Writing – review & editing. Tom Oomen: Conceptualization, Data curation, Formal analysis, Funding acquisition, Investigation, Methodology, Project administration, Resources, Software, Supervision, Validation, Visualization, Writing – original draft, Writing – review & editing.

#### **Declaration of competing interest**

The authors declare that they have no known competing financial interests or personal relationships that could have appeared to influence the work reported in this paper.

#### Data availability

The authors are unable or have chosen not to specify which data has been used.

#### Acknowledgments

The authors would like to thank TNO, and in particular Max Baeten, Robbert Voorhoeve, and Stefan Kuiper, for the developments that have led to these results, for their valuable inputs and ideas, and their help and support in carrying out the experiments reported in this paper.

#### Appendix. Proof of Theorem 2

**Proof.** Let  $R_k$  be a rank-one modal participation matrix and  $\rho_{s,ps,i} = \rho_{s,bp,j} = \rho_{a,k}$  for any  $i,j,l \in \mathbb{N}$  be the collocated positions of the sensor-actuator triplet. As such, the mass-normalized mode shape vectors are related through

$$[v_{ps,k}]_i - [v_{ps,k}]_i = [w_k]_i.$$
 (A.1)

By virtue of Theorem 1, the rank-one modal participation matrix can be decomposed into a dyadic product of mode shape vectors  $\tilde{v}_{ps,k}$ ,  $\tilde{v}_{bp,k}$ , and  $\tilde{w}_k$  which are unique up to a scaling parameter  $\beta$ 

$$R_k = \begin{bmatrix} \beta \tilde{v}_{\text{ps},k} \\ \beta \tilde{v}_{\text{bp},k} \end{bmatrix} \frac{1}{\beta} \tilde{w}_k^{\top}. \tag{A.2}$$

These mode shape vectors are mass-normalized by finding the scaling parameter  $\beta^*$  such that

$$\begin{bmatrix} v_{\text{ps},k} \\ v_{\text{bp},k} \end{bmatrix} = \begin{bmatrix} \beta^* \tilde{v}_{\text{bp},k} \\ \beta^* \tilde{v}_{\text{bp},k} \end{bmatrix} \qquad w_k = \beta^* \tilde{w}_k$$
(A.3)

Substitution of (A.1) in (A.3) and subsequent reformulation leads to the scaling parameter

$$\beta^* = \sqrt{\frac{[w_{\text{bp},k}]_i}{[v_{\text{ps},k}]_j - [v_{\text{bp},k}]_l}}$$
(A.4)

which mass-normalizes any arbitrarily scaled mode shape vectors  $\tilde{v}_{\mathrm{ps},k}$ ,  $\tilde{v}_{\mathrm{bp},k}$ , and  $\tilde{w}_k$  and completes the proof of Theorem 2.  $\square$ 

#### References

- [1] Kuiper S, Doelman N, Human J, Saathof R, Klop W, Maniscalco M. Advances of TNO's electromagnetic deformable mirror development. In: Advances in optical and mechanical technologies for telescopes and instrumentation, vol. 10706, SPIE; 2018, p. 345–52.
- [2] Beckers JM. Adaptive optics for astronomy: principles, performance, and applications. Ann Rev Astron Astrophys 1993;31(1):13-62.
- [3] Roddier F. Adaptive optics in astronomy. Cambridge University Press; 1999.
- [4] Yu C, Verhaegen M. Structured modeling and control of adaptive optics systems. IEEE Trans Control Syst Technol 2017;26(2):664–74.
- [5] Rimmele TR. Recent advances in solar adaptive optics. In: Advancements in adaptive optics, vol. 5490, SPIE; 2004, p. 34–46.
- [6] Steinbuch M, Oomen T, Vermeulen H. Motion control, mechatronics design, and moore's law. IEEE J Ind Appl 2022;11(2):245–55.
- [7] Gasmi R, Le Bihan D, Dournaux J-L, Sinquin J, Jagourel P. Active control of a large deformable mirror for future E-ELT. In: Adaptive optics systems, vol. 7736, SPIE; 2010, p. 505–15.
- [8] Neureuther PL, Schmidt K, Bertram T, Sawodny O. Control oriented modelling and modal analysis of the deformable mirror M4 of the extremely large telescope. Math Comput Model Dyn Syst 2021;27(1):295–321.
- [9] Haber A, Bifano T. General approach to precise deformable mirror control. Opt Express 2021;29(21):33741–59.
- [10] Hamelinck R, Ellenbroek R, Rosielle N, Steinbuch M, Verhaegen M, Doelman N. Validation of a new adaptive deformable mirror concept. In: Adaptive optics systems, vol. 7015. SPIE: 2008, p. 163–74.
- [11] Balas GJ, Doyle JC. Control of lightly damped, flexible modes in the controller crossover region. J Guid Control Dyn 1994;17(2):370–7.
- [12] Oomen T, van Herpen R, Quist S, van de Wal M, Bosgra O, Steinbuch M. Connecting system identification and robust control for nextgeneration motion control of a wafer stage. IEEE Trans Control Syst Technol 2014;22(1):102–18.
- [13] Tyson RK, Byrne DM. The effect of wavefront sensor characteristics and spatiotemporal coupling on the correcting capability of a deformable mirror. In: Active optical devices and applications, vol. 228, SPIE; 1980, p. 21–5.
- [14] Chiuso A, Muradore R, Marchetti E. Dynamic calibration of adaptive optics systems: A system identification approach. IEEE Trans Control Syst Technol 2009;18(3):705–13.
- [15] Toporovsky V, Kudryashov A, Skvortsov A, Rukosuev A, Samarkin V, Galaktionov I. State-of-the-art technologies in piezoelectric deformable mirror design. In: Photonics. MDPI; 2022, p. 321.
- [16] Coronel M, Soto N, Carvajal R, Escárate P, Agüero JC. Identification and model predictive control of an experimental adaptive optics setup utilizing Kautz basis functions. In: Adaptive optics systems VII, vol. 11448, SPIE; 2020, p. 497–508.
- [17] Kilpatrick J, Apostol A, Khizhnya A, Markov V, Beresnev L. Realtime characterization of the spatio-temporal dynamics of deformable mirrors. In: Laser communication and propagation through the atmosphere and oceans V, vol. 9979, SPIE; 2016, p. 34-45.
- [18] Markov V, Khizhnyak A, Kilpatrick J, Morrison P, Osborne G, Siegenthaler J, et al. Characterization of spatio-temporal dynamics of deformable mirrors. In: Laser communication and propagation through the atmosphere and oceans VII, vol. 10770, SPIE; 2018, p. 97–107.
- [19] Gasmi R, Dournaux J, Cousty R, Le Bihan D, Crépy B, Jagourel P. Numerical and experimental modal analysis of a 1-meter deformable mirror. In: Proc. ISMA noise and vibration engineering. 2010.
- [20] Oya S, Bouvier A, Guyon O, Watanabe M, Hayano Y, Takami H, et al. Performance of the deformable mirror for Subaru LGSAO. In: Advances in adaptive optics II, vol. 6272, SPIE; 2006, p. 1523–30.
- [21] Haber A, Verhaegen M. Modeling and state-space identification of deformable mirrors. Opt Express 2020;28(4):4726–40.
- [22] Ruppel T, Osten W, Sawodny O. Model-based feedforward control of large deformable mirrors. Eur J Control 2011;17(3):261–72.
- [23] Ruppel T, Dong S, Rooms F, Osten W, Sawodny O. Feedforward control of deformable membrane mirrors for adaptive optics. IEEE Trans Control Syst Technol 2012;21(3):579–89.
- [24] Vogel CR, Tyler GA, Lu Y. Modeling, parameter estimation, and open-loop control of MEMS deformable mirrors. In: MEMS adaptive optics IV, vol. 7595, SPIE; 2010, p. 101–6.
- [25] Vogel C, Tyler G, Lu Y, Bifano T, Conan R, Blain C. Modeling and parameter estimation for point-actuated continuous-facesheet deformable mirrors. J Opt Soc Amer A 2010;27(11):A56–63.
- [26] Morzinski KM, Harpsøe KB, Gavel DT, Ammons SM. The openloop control of MEMS: modeling and experimental results. In: MEMS adaptive optics, vol. 6467, SPIE; 2007, p. 129–38.
- [27] Pintelon R, Schoukens J, Vandersteen G, Barb'e K. Estimation of nonparametric noise and FRF models for multivariable systems—Part II: extensions, applications. Mech Syst Signal Process 2010;24(3):596–616.
- [28] Oomen T. Advanced motion control for precision mechatronics: Control, identification, and learning of complex systems. IEEE J Ind Appl 2018;7(2):127–40.

- [29] Voorhoeve R, de Rozario R, Aangenent W, Oomen T. Identifying position-dependent mechanical systems: A modal approach applied to a flexible wafer stage. IEEE Trans Control Syst Technol 2020;29(1):194–206.
- [30] Pintelon R, Schoukens J. System identification: a frequency domain approach. John Wiley & Sons: 2012.
- [31] Voorhoeve R, van der Maas A, Oomen T. Non-parametric identification of multivariable systems: A local rational modeling approach with application to a vibration isolation benchmark. Mech Syst Signal Process 2018;105:129–52.
- [32] Evers E, van Tuijl N, Lamers R, de Jager B, Oomen T. Fast and accurate identification of thermal dynamics for precision motion control: Exploiting transient data and additional disturbance inputs. Mechatronics 2020;70:102401.
- [33] Peumans D, De Vestel A, Busschots C, Rolain Y, Pintelon R, Vandersteen G. Accurate estimation of the non-parametric FRF of lightlydamped mechanical systems using arbitrary excitations. Mech Syst Signal Process 2019;130:545–64.
- [34] Pintelon R, Schoukens J, Guillaume P. Parametric frequency domain modeling in modal analysis. Mech Syst Signal Process 1989;3(4):389–403.
- [35] Chen N, Potsaid B, Wen JT, Barry S, Cable A. Modeling and control of a fast steering mirror in imaging applications. In: 2010 IEEE international conference on automation science and engineering. IEEE; 2010, p. 27–32.
- [36] Noël J-P, Renson L, Kerschen G, Peeters B, Manzato S, Debille J. Nonlinear dynamic analysis of an F-16 aircraft using GVT data. In: International forum on aeroelasticity and structural dynamics. 2013, p. 990–1002.
- [37] Keas P, Brewster R, Guerra J, Lampater U, Kärcher H, Teufel S, Wagner J. SOFIA telescope modal survey test and test-model correlation. In: Modeling, systems engineering, and project management for astronomy IV, vol. 7738, SPIE; 2010, p. 207–32
- [38] Pappalardo CM, Guida D. Development of a new inertial-based vibration absorber for the active vibration control of flexible structures. Eng Lett 2018;26(3).
- [39] Betti E. Teoria della elasticita. Il Nuovo Cimento (1869-1876) 1872;7(1):291-378.
- [40] Maxwell JC. On the calculation of the equilibrium and stiffness of frames. Phil Mag J Sci 1864;27(182):598–604.
- [41] Gawronski WK. Dynamics and control of structures: a modal approach. Springer Science & Business Media; 2004.
- [42] Tacx P, Teurlings M, Habraken R, Witvoet G, Heertjes M, Oomen T. Spatio-temporal analysis of overactuated motion systems: A mechanical modeling approach. In: IFAC world congress. 2023, p. 8784–90.
- [43] Van de Wal M, van Baars G, Sperling F, Bosgra O. Multivariable H<sub>∞</sub>/μ feedback control design for high-precision wafer stage motion. Control Eng Practice 2002:10(7):739–55.
- [44] Dalimier E, Dainty C. Comparative analysis of deformable mirrors for ocular adaptive ontics. Ont Express 2005;13(11):4275–85
- [45] Chun M, Baranec C, Lai O, Lu JR, Zhang R, Kuiper S, et al. A new adaptive secondary mirror for astronomy on the University of Hawaii 2.2-meter telescope. In: Adaptive optics systems VII, vol. 11448, SPIE; 2020, p. 292–9.
- [46] Levy E. Complex-curve fitting. IRE Trans Autom Control 1959;4(1):37–43.
- [47] Li H-X, Qi C. Modeling of distributed parameter systems for applications— A synthesized review from time-space separation. J Process Control 2010;20(8):891–901.
- [48] Tacx P, Oomen T. Accurate  $H_{\infty}$ -norm estimation via finite-frequency norms of local parametric models. In: American control conference. IEEE; 2021, p. 332–7.
- [49] Reynders E. System identification methods for (operational) modal analysis: review and comparison. Arch Comput Methods Eng 2012;19(1):51–124.
- [50] Axler S. Linear algebra done right. Springer Science & Business Media; 1997.
- [51] Shores TS, et al. Applied linear algebra and matrix analysis, vol. 2541, Springer; 2007.
- [52] Richardson MH, Jamestown C. Modal mass, stiffness and damping. Jamestown, CA: Vibrant Technology, Inc.; 2000, p. 1–5.
- [53] Keller W, Borkowski A. Thin plate spline interpolation. J Geod 2019;93:1251–69.



Paul Tacx received the M.Sc. degree (cum laude) in mechanical engineering from the Eindhoven University of Technology, Eindhoven, the Netherlands, in 2019, where he is currently pursuing the Ph.D. degree in the Control Systems Technology Group. His research interests include identification for advanced motion control and control of complex mechatronic systems.



Roel Habraken received the M.Sc. degree in mechanical engineering from the Eindhoven University of Technology, Eindhoven, the Netherlands, in 2022. He is currently working as a mechanical design engineer at Prodrive Technologies in the fields of motion control and precision design for mechatronic systems.



Gert Witvoet received the M.Sc. (cum laude) and Ph.D. degrees from the Eindhoven University of Technology, Eindhoven, The Netherlands, in 2007 and 2011, respectively. He is currently a Senior Dynamics and Control Specialist at the Netherlands Organization for Applied Scientific Research (TNO), Delft, The Netherlands, and a part-time Associate Professor with the Mechanical Engineering Department, Eindhoven University of Technology. His research interest includes the application of advanced motion control techniques on high-tech instruments and applications in the semiconductor, astronomy, and space markets. Dr. Witvoet is a recipient of the Unilever Research Prize and several best master teacher awards.



Marcel Heertjes received the M.Sc. and Ph.D. degrees from the Eindhoven University of Technology, Eindhoven, The Netherlands, in 1995 and 1999, respectively. After being with the Philips Center for Industrial Technology from 20002005, he joined ASML in 2006. He was a recipient of the IEEE Control Systems Technology Award 2015 for variable gain control and its applications to wafer scanners. In 2019, he was appointed full Professor on Industrial Nonlinear Control for High-Precision Systems at Eindhoven University of Technology. He acts as an Associate Editor for IFAC Mechatronics since 2016. Regarding his work on hybrid integrator-gain systems, he was a recipient of the IFAC Automatica paper prize award 2023.



Tom Oomen is full professor with the Department of Mechanical Engineering at the Eindhoven University of Technology. He is also a part-time full professor with the Delft University of Technology. He received the M.Sc. degree (cum laude) and Ph.D. degree from the Eindhoven University of Technology, Eindhoven, The Netherlands. He held visiting positions at KTH, Stockholm, Sweden, and at The University of Newcastle, Australia. He is a recipient of the 7th Grand Nagamori Award, the Corus Young Talent Graduation Award, the IFAC 2019 TC 4.2 Mechatronics Young Research Award, the 2015 IEEE Transactions on Control Systems Technology Outstanding Paper Award, the 2017 IFAC Mechatronics Best Paper Award, the 2019 IEEJ Journal of Industry Applications Best Paper Award, and recipient of a Veni and Vidi personal grant. He is currently a Senior Editor of IEEE Control Systems Letters (L-CSS) and Associate Editor of IFAC Mechatronics, and he has served on the editorial boards of the IEEE Control Systems Letters (L-CSS) and IEEE Transactions on Control Systems Technology. He has also been vice-chair for IFAC TC 4.2 and a member of the Eindhoven Young Academy of Engineering. His research interests are in the field of data-driven modeling, learning, and control, with applications in precision mechatronics.